Showcasing research from the Kou-Lin Zhang lab at School of Chemistry and Chemical Engineering, Yangzhou University.

A novel photoluminescent Cd(II)–organic framework exhibiting rapid and efficient multi-responsive fluorescence sensing for trace amounts of Fe^{3+} ions and some NACs, especially for 4-nitroaniline and 2-methyl-4-nitroaniline

A novel Cd(II)–organic framework which shows distinct solvent-dependent fluorescence and multi-responsive sensing behavior for Fe^{3+} ions and some NACs, especially for 4-NA and 2-M-4-NA, has been rationally designed and successfully constructed.

As featured in:

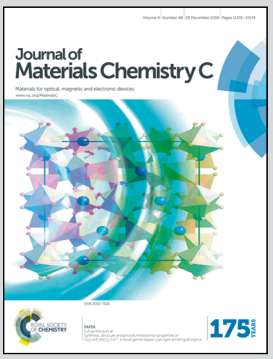

See Kou-Lin Zhang *et al.*, *J. Mater. Chem. C*, 2016, **4**, 11404.

ROYAL SOCIETY OF CHEMISTRY

www.rsc.org/MaterialsC

Registered charity number: 207890

Journal of Materials Chemistry C

PAPER

Cite this: J. Mater. Chem. C, 2016, 4, 11404

A novel photoluminescent Cd(II)–organic framework exhibiting rapid and efficient multi-responsive fluorescence sensing for trace amounts of Fe^{3+} ions and some NACs, especially for 4-nitroaniline and 2-methyl-4-nitroaniline†

Ying-Jiao Yang,‡ Meng-Jie Wang‡ and Kou-Lin Zhang*

Received 26th September 2016,
Accepted 7th November 2016

DOI: 10.1039/c6tc04195g

www.rsc.org/MaterialsC

The first photoluminescent Cd(II)–organic framework $\{[Cd(5\text{-asba})(bimb)]\}_n$ (**1**) based on a multi-functional ligand, 2-amino-5-sulfobenzoic acid ($H_2$5-asba), has been successfully constructed. The structure of **1** was determined by single crystal X-ray diffraction analysis, revealing that **1** exhibits a six-connected α-polonium network with a Schläfli symbol of $4^{12}\cdot6^3$. The phase purity of the bulk sample of **1** was further confirmed by elemental analysis and powder X-ray diffraction pattern (PXRD) which was consistent with the simulated phase purity calculated from single crystal X-ray diffraction data. The optical property of **1** was characterized by analysis of the solid state UV-vis diffuse reflectance spectrum, indicating that **1** may be a potential candidate for wide gap semiconductor materials. The photoluminescence properties of **1** well dispersed in various solvents have been investigated in detail, indicating that **1** shows distinct solvent-dependent photoluminescence. **1** belongs to the rare category of MOFs that exhibit multi-responsive photoluminescence sensing properties. It can be used as a rapid and efficient selective fluorescent sensor for Fe^{3+} ions in environmental and biological systems at about a one ppm level. For the photoluminescence responses of **1** dispersed in aqueous solution with incrementally increased 4-nitroaniline (4-NA) and 2-methyl-4-nitroaniline (2-M-4-NA) concentrations, photoluminescence quenching was detectable even at a very low concentration of 0.52 ppm for 4-NA and 0.68 ppm for 2-M-4-NA, indicating that **1** exhibits extremely high sensitivities for 4-NA and 2-M-4-NA. A further systematic study reveals that **1** shows more efficient sensing of nitroaniline homologues (4-NA and 2-M-4-NA) over other electron-deficient nitroaromatic compounds (NACs). **1** represents the first case of a MOF-based photoluminescent probe for 4-NA and 2-M-4-NA. Furthermore, **1** can discriminate the nitrophenol isomers (2-, 3- and 4-NP) through fluorescence sensing. To our best knowledge, **1** is the first Cd(II) MOF based on the multi-functional ligand $H_2$5-asba that can be used as a multi-responsive efficient sensory material for Fe^{3+} ions and some NACs, especially for nitroaniline homologues (4-NA and 2-M-4-NA).

Introduction

Iron is one of the most important elements in the daily metabolic process of almost all mammals. However, either a deficiency or excess of iron from normal permissible limits can lead to serious disorders.[1] Some valuable analytical techniques, such as voltammetry,[2] spectrophotometry,[3] atomic absorption spectroscopy,[4] and inductively coupled plasma (ICP) mass spectrometry,[5] have been used for the determination of Fe^{3+} ions, but some metal ions were found to interfere with the measurements, which leads to complicated pretreatment, high cost and sophisticated machines. Therefore, the rapid and selective detection of trace amounts of Fe^{3+} ions in both environmental and biological areas at low cost is very important. Recently, chemists have had much interest in the use of the fluorescent property of MOFs for the sensing of small molecules and metal ions, which may result from the diverse topologies and functional recognition sites in MOFs.[6–9] However, only limited novel work has been dedicated to the design and synthesis of sensitive MOF-based fluorescent sensors for Fe^{3+} ions.[9]

School of Chemistry and Chemical Engineering, Yangzhou University, Yangzhou 225002, P. R. China. E-mail: koulinzhang2002@yahoo.com; Fax: +86 514 87975244; Tel: +86 514 87975244

† Electronic supplementary information (ESI) available. CCDC 855376 (**1**). For ESI and crystallographic data in CIF or other electronic format see DOI: 10.1039/c6tc04195g

‡ Y.-J. Yang and M.-J. Wang contributed equally.

On the other hand, with the rapid development of the chemical industry and extensive use of pesticides in agriculture, chemicals such as some nitroaromatic compounds (NACs) have become serious pollution sources in groundwater, soil and other security applications due to their high toxicity and the detriment caused to sustainable development and human health.[10] Currently, how to solve pollution problems has become one of the most popular topics worldwide. So, convenient and efficient technologies for detecting NACs in the environment have received much attention from chemists. Some traditional instrumental techniques, such as chromatography, gas metal detectors and cyclic voltammetry, *etc.*, have high efficiency, but they usually need very expensive instruments, and in most of cases they aren't easily accessible and have inconvenient processes.[11] Therefore, new technologies need to be developed so that we can obtain rapid detection at low cost. Fluorescence-based sensing materials have recently been considered as one of the most excellent and promising techniques in the detection of NACs because this kind of technique possesses several advantages such as high efficiency, selectivity and simplicity.[12,13]

During the past years, polymeric, oligomeric or photoluminescent nanoscale materials have been rationally designed and constructed successfully for the determination of some NACs.[14] But, it is still a great challenge for chemists to design and prepare novel fluorescent materials for the detection of NACs because it isn't easy to introduce fluorophores into the above-mentioned fluorescent sensors. Compared with traditional metal–inorganic materials, metal–organic frameworks (MOFs) are a new class of developing metal–organic hybrid functional materials, which can be built from metal cations and organic ligands and have extensive potential applications in gas storage, photoactive materials, drug delivery, magnetic materials, separations and chemical sensors, *etc.*[15] The fluorescence behavior of a MOF is highly dependent on organic ligands and metal ions. Thus, it is relatively easy to construct fluorescent MOFs by using either organic ligands with fluorophores or metal ions, such as d^{10} metal ions (Zn^{2+}, Cd^{2+}) or Ln^{3+}, or utilizing a combination of these two parts.[16] For example, a novel Zn(II) MOF exhibiting rapid and reversible detection of high explosives was first reported in 2009.[17] The Su group constructed a novel Cd(II) MOF that can recognize NACs with different numbers of nitro groups.[18] Two novel Ln(III) MOFs as efficient photoluminescent sensors for explosive 2,4,6-trinitrophenol have been reported by two independent groups.[19] The Zheng group reported two novel photoluminescent Zn(II) MOFs for efficient selective sensing of picric acid.[20]

4-nitroaniline (4-NA) is mainly used as an intermediate of fine chemicals, such as pesticides, pharmaceuticals and dyes, *etc.*; 2-methyl-4-nitroaniline (2-M-4-NA) is chiefly used for the dyeing and printing of cotton and ramie fabric, and it is also used in the production of paint. However, both are extremely harmful to aquatic organisms and may cause long-term adverse effects on the aquatic environment. So, detecting these pollutants in the environment, especially in waste water, rapidly and conveniently is a popular topic for chemists. Although MOFs have been reported for the efficient sensing of some nitroaromatics and inorganic ions, *etc.*, there is still no report available in the literature on the rapid and efficient sensing of trace amounts of nitroaniline homologues by a MOF material.

According to the analysis of reported novel MOF-based fluorescent sensors, from a rational design point of view, the framework (receptor unit) should better contain an aromatic ring with a nonbonded functional site that has the potential to interact with the analyte (substrate) selectively and efficiently, and also the receptor unit is usually connected to a suitable fluorophore unit that can generate a distinct emission upon recognition. Once the analyte is recognized by the receptor, the fluorescence responses can be observed in the form of quenching (turn off) or enhancement (turn on) in the emission intensity due to charge transfer, energy transfer or electron donor–acceptor transfer mechanisms.[21]

Recently, we are focusing our attention on selecting 2-amino-5-sulfobenzoic acid ($H_2$5-asba) as the organic moiety (Scheme 1) to attempt to construct sensitive MOF-based fluorescent sensors for chemical pollutants such as metal ions and NACs, which is based mostly on the following considerations: (1) the carboxylate, sulfonate and amino groups in the electron-rich ligand 5-asba^{2-} are potential interaction sites to recognize the analyte (NACs) efficiently through hydrogen bonds. Furthermore, according to the "Hard–soft acid base (HSAB)" theory, the electron-rich sulfonate group belongs to the "Hard base" and has the potential to form strong $(-S_{sulfonate}O_3)^{-}\cdots M^{n+}$ electrostatic interactions with hard metal ions such as Fe^{3+}, *etc.*; (2) as an anionic aromatic carboxylate ligand, 5-asba^{2-} can connect to a suitable fluorophore unit that produces a distinct fluorescence intensity change upon recognition with the analyte; (3) rich binding modes of the ligand 5-asba^{2-} are anticipated under appropriate reaction conditions, which will provide new insights to construct "building blocks" for the construction of specific coordination assemblies. To our best knowledge, there are still no MOFs reported with the multi-functional ligand $H_2$5-asba so far.

Herein, we report a novel photoluminescent Cd(II)–organic framework sensory material based on $H_2$5-asba {[Cd(5-asba)(bimb)]}$_n$ (**1**) [bimb = 1,4-bis(1*H*-imidazol-1-yl)butane], exhibiting a 3D α-polonium network with symbol $4^{12}\cdot6^3$. **1** shows distinct solvent-dependent fluorescence and rapid selective fluorescence sensing of trace amounts of Fe^{3+} ions in environmental and biological systems. Remarkably, **1** can also be used as a rapid and efficient fluorescent sensor for some NACs, especially for nitroaniline homologues (4-NA and 2-M-4-NA) (Scheme 2). So, the present MOF shows the multi-responsive sensing behavior of

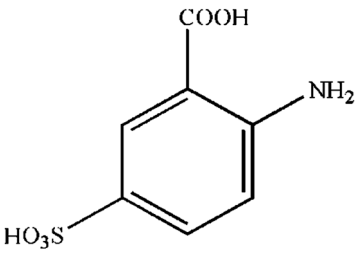

Scheme 1

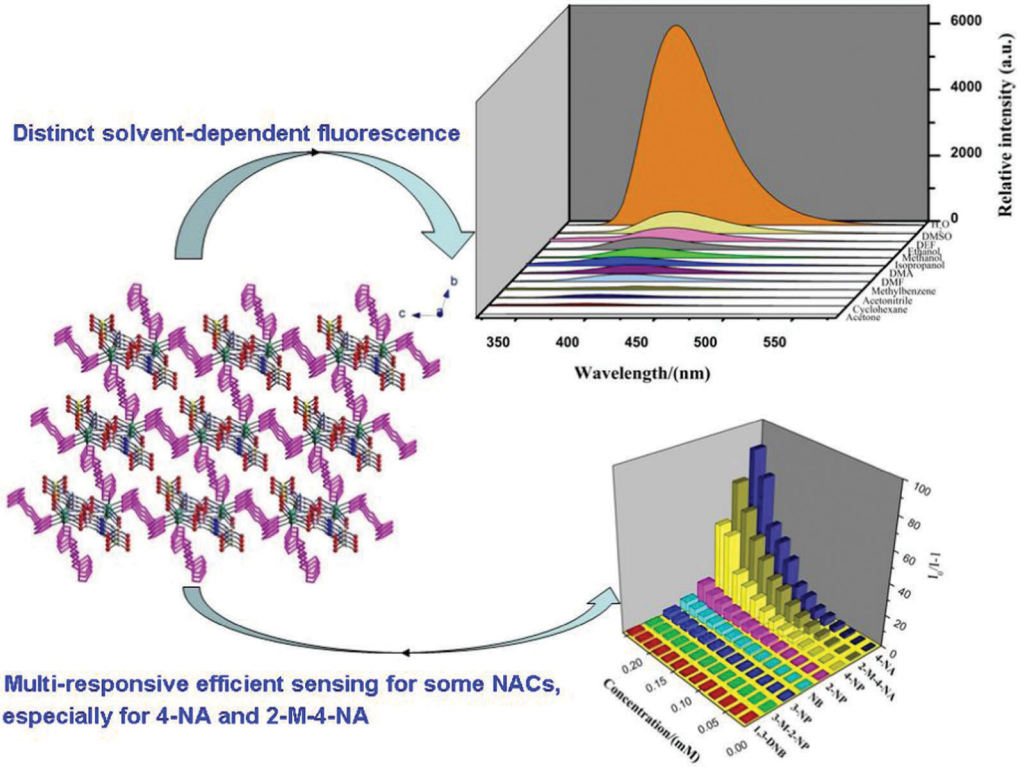

Scheme 2 Simplified diagram showing the distinct solvent-dependent photoluminescence and multi-responsive sensing behavior of the Cd(II) MOF for some NACs, especially for nitroaniline homologues (4-NA and 2-M-4-NA).

rapid and efficient detection of trace amounts of nitroaniline homologues and Fe^{3+} ions. The detection limits to Fe^{3+} ions, 4-NA and 2-M-4-NA reach at least one ppm, 0.52 ppm and 0.68 ppm levels, respectively. Moreover, to our best knowledge, **1** is the first reported MOF-based sensory material that can discriminate nitrophenol isomers (2-, 3- and 4-NP) through fluorescence sensing.

Results and discussion

Crystal structure description

Single crystal X-ray structural analysis shows that MOF **1** crystallizes in the triclinic system with the space group $P\bar{1}$ (Table 1). The asymmetric unit consists of one crystallographic independent Cd(II) ion, one 5-asba^{2-} anion and one bimb ligand. Each six-coordinated Cd(II) ion is bound by three N atoms: two N atoms from the two bimb ligands and one from the amino group of the ligand 5-asba^{2-}, and three oxygen atoms: one from the sulfonate group and the other two from the carboxylate group of 5-asba^{2-}, and exhibits a distorted octahedral coordination geometry with subtended angles ranging from 54.48(9) to 157.79(11)° (Fig. 1A and Table 2). The carboxylate group in the ligand 5-asba^{2-} exhibits chelating conformation, and the amino group also coordinates with the central Cd(II) atom, resulting in the formation of two kinds of alternatively arranged centrosymmetrical 5-asba^{2-}-bridged dinuclear units [Cd_2(asba)$_2$], which are further linked with each other through the monodentate sulfonate group, resulting in a 5-asba^{2-}-bridged chain, which acts as the secondary building unit (SBU) (Fig. 1B). The nearest Cd···Cd separation within the chain is 6.2100(6) Å. So, the ligand 5-asba^{2-} adopts a (k^1–k^1)–(k^1)–(k^1)-μ_3 coordination mode (Fig. 1C). The SBUs are further connected by the bimb

Table 1 Crystallographic data and structure refinement details for **1**

Empirical formula	$C_{17}H_{19}CdN_5O_5S$
Formula weight	517.83
Wavelength (Å)	0.71073
Crystal system	Triclinic
Space group	$P\bar{1}$
a (Å)	8.6563(9)
b (Å)	9.0640(9)
c (Å)	13.2673(13)
α (°)	106.6200(10)
β (°)	92.7750(10)
γ (°)	100.4390(10)
Volume (Å^3)	975.40(17)
Z	2
Density (mg m^{-3})	1.763
Absorption coeff. (mm^{-1})	1.267
F(000)	520
θ range for data collection (°)	1.61 to 25.00
Index ranges	$-10 \le h \le 10$, $-10 \le k \le 10$, $-15 \le l \le 15$
Reflections collected	6992
Unique	3417
R_{int}	0.0359
Completeness to θ	99.10%
Max. and min. transmission	0.701 and 0.673
Goodness-of-fit on F^2	1.075
Final R indices [$I > 2\sigma(I)$]	R_1 = 0.0383, wR_2 = 0.1043
R indices (all data)	R_1 = 0.0390, wR_2 = 0.1050
Largest diff. peak and hole (e Å^{-3})	1.753 and −2.001

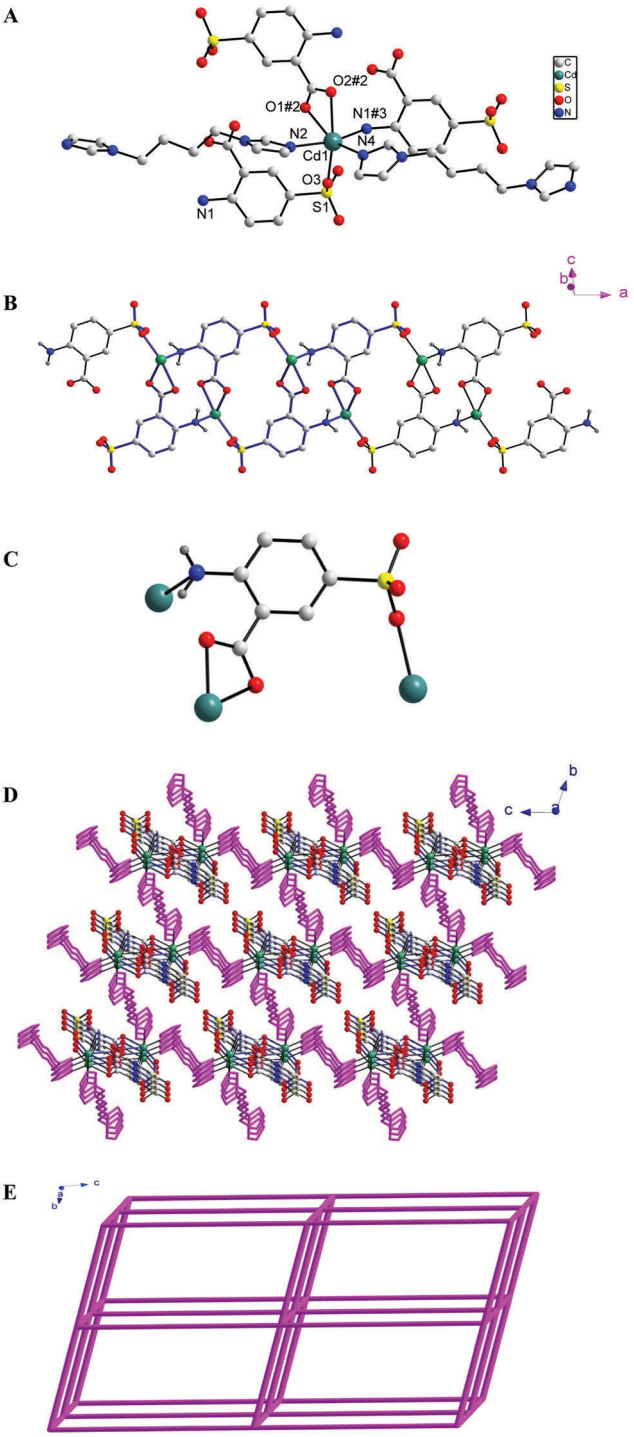

Fig. 1 (A) Coordination environment of the Cd(II) ion in **1**, also showing the *trans–trans–trans* conformation of bimb. Symmetry codes: #2 $-x+2$, $-y+1$, $-z+1$ #3 $x-1$, y, z. (B) View of the 5-asba^{2-}-bridged chain (SBU). (C) The coordination mode $(k^1\text{–}k^1)\text{–}(k^1)\text{–}(k^1)\text{-}\mu_3$ of 5-asba^{2-} in **1**. (D) The SBUs are further connected by the bimb ligand, resulting in a 3D framework. (E) Schematic representation of the 3D α-Po topological network.

ligands in *trans–trans–trans* conformation, leading to the formation of 3D framework architecture.

From a topological point of view, if the pseudo atoms inserted in the carboxylate-bridged dinuclear units are treated as nodes and the distances between the nearest pseudo atoms as linkers, the framework of **1** can be simplified as a 3D α-polonium network with the Schläfli symbol $(4^{12}\cdot6^3)$ (Fig. 1D and E).

Table 2 Selected bond lengths (Å) and angles (°) for **1**

Cd(1)–N(4)	2.250(4)	Cd(1)–O(3)	2.277(3)
Cd(1)–N(2)	2.299(4)	Cd(1)–O(2)#1	2.377(3)
Cd(1)–N(1)#4	2.458(3)	Cd(1)–O(1)#1	2.456(3)
N(4)–Cd(1)–O(3)	100.53(13)	N(4)–Cd(1)–N(2)	100.02(15)
O(3)–Cd(1)–N(2)	92.81(15)	N(4)–Cd(1)–O(2)#1	100.65(12)
O(3)–Cd(1)–O(2)#1	157.79(11)	N(2)–Cd(1)–O(2)#1	90.05(15)
N(4)–Cd(1)–O(1)#1	155.11(12)	O(3)–Cd(1)–O(1)#1	104.08(10)
N(2)–Cd(1)–O(1)#1	82.55(13)	O(2)#1–Cd(1)–O(1)#1	54.48(9)
N(4)–Cd(1)–N(1)#4	100.78(13)	O(3)–Cd(1)–N(1)#4	85.64(11)
N(2)–Cd(1)–N(1)#4	159.07(14)	O(2)#1–Cd(1)–N(1)#4	83.90(11)
O(1)#1–Cd(1)–N(1)#4	77.62(11)		

FT-IR spectrum and thermal stability

The FT-IR spectral data show features attributable to the carboxylate characteristic stretching vibrations of **1** (Fig. S1, ESI†). The absence of bands in the range of 1680–1760 cm^{-1} reveals the complete deprotonation of $H_2$5-asba in **1**. The characteristic bands of the carboxylate groups are located at 1611 cm^{-1} for asymmetric stretching and 1535 cm^{-1} for symmetric stretching. The characteristic stretching vibration of the sulfonate group in **1** is located at 1180 cm^{-1}. The strong bands centered on 3301 cm^{-1} and 3233 cm^{-1} correspond to the stretching vibrations of the –NH_2 group in **1**.[22]

To study the thermal stability of MOF **1**, thermogravimetric analysis (TGA) was performed under a N_2 atmosphere in flowing N_2 at a heating rate of 10 °C min^{-1}. No weight loss is observed below 356 °C in the TG curve of **1**, which further confirms the absence of water molecules in the bulk sample of **1**. **1** decomposes at 356 °C, revealing that the framework of **1** has a high thermal stability (Fig. 2).

Optical energy gap

The solid state diffuse reflectance UV-vis spectra at room temperature were recorded for the as-synthesized sample of **1**,

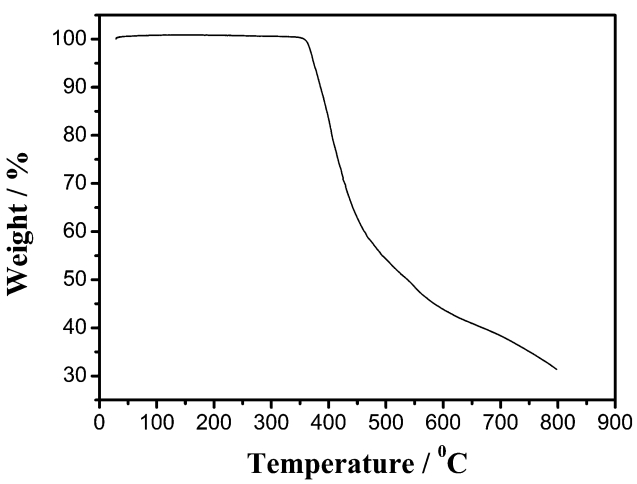

Fig. 2 TG curve of **1**.

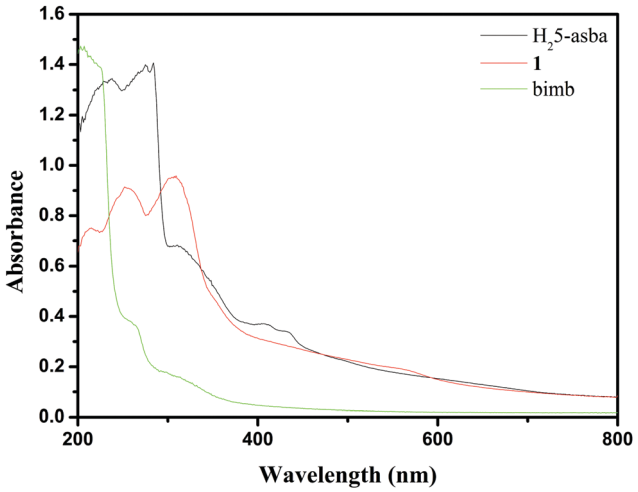

Fig. 3 The solid state diffuse UV-vis reflectance spectra for $H_2$5-asba (black), bimb (green) and **1** (red).

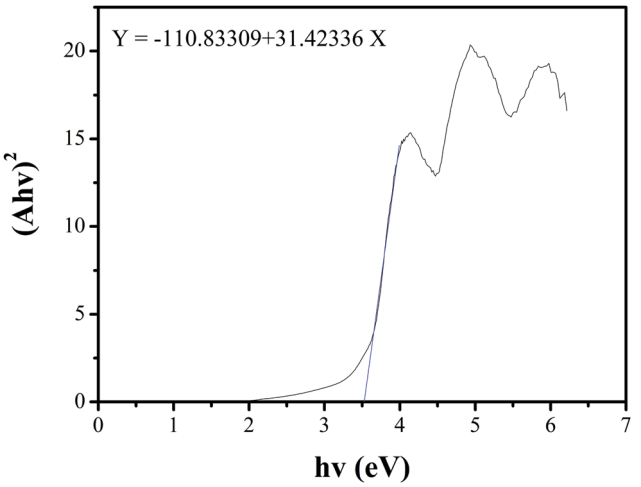

Fig. 4 Diffuse reflectance UV-vis spectrum of $(Ah\nu)^2$ *vs.* photon energy ($h\nu$) for **1**.

$H_2$5-asba and bimb (Fig. 3). We took a more detailed analysis of the UV-vis spectra of bimb, $H_2$5-asba and MOF **1** in order to know which peaks of MOF **1** belong to which ligand. There are two peaks in the UV-vis spectrum of bimb: one around 200 nm and another at 261 nm, which can be attributed to the π → π* and n → π* transitions, respectively.[23a,b] Several peaks appear in the spectrum of $H_2$5-asba: the peaks at 236 and 276 nm can be attributed to the phenyl π → π* transition, while the weak peaks around 312 and 400 nm can be ascribed to the n → π* transition of the ligand $H_2$5-asba.[23a,b] There are three peaks in the spectrum of MOF **1**: 215, 255 and 305 nm. It is worth pointing out that the n → π* transitions of the free ligands bimb and $H_2$5-asba cannot appear in the UV-vis spectrum of MOF **1** since these ligands coordinate with the central Cd(II) ions simultaneously. Therefore, the peaks at 255 and 305 nm can be ascribed to the phenyl π → π* transition of the ligand 5-asba^{2-} and the peak at 215 nm to the π → π* transition of bimb.[23] The slightly red shifts of the absorption bands in **1** may be attributed to the coordination effect of the ligand 5-asba^{2-}, resulting in a relatively large delocalization effect.[24]

Scientists have documented that a common and convenient method for determining whether a band gap is indirect or direct is to use UV-vis absorption analysis.[25] Accordingly, to study the conductivity of MOF **1**, the solid state diffuse reflectance UV-vis spectrum of **1** was applied to calculate the band gap E_g, which was determined as the intersection point between the energy axis ($h\nu$) and the line derived from the linear portion of the absorption edge in a plot of the K–M (Kubelka–Munk) function F *vs.* the incident photon energy $h\nu$. If a plot of $(Ah\nu)^2$ *vs.* photon energy ($h\nu$) results in a straight line, it can normally be inferred that there is a direct band gap. On the other hand, if a plot of $(Ah\nu)^{1/2}$ *vs.* photon energy ($h\nu$) results in a straight line, it can usually be inferred that the band gap is indirect. Therefore, to judge if the band gap of MOF **1** is direct or indirect, we firstly draw two corresponding plots. We found that the plot of $(Ah\nu)^2$ *vs.* $h\nu$ (Fig. 4) has better linearity than that of $(Ah\nu)^{1/2}$ *vs.* $h\nu$ (Fig. S2, ESI†). So, the band gap E_g of MOF **1** can be determined based on the theory of optical absorption for a direct band gap semiconductor: $(Ah\nu)^2 = B(h\nu - E_g)$, where B is a constant corresponding to the material itself. The E_g value derived from the steep absorption edge is 3.53 eV, indicating the existence of an optical direct band gap and the characteristic of semiconductivity for MOF **1**. Therefore, MOF **1** may be used as a potential wide gap semiconductor material.[25]

Fluorescent property of MOF 1 in the solid state

It has been documented that MOFs with d^{10} metal ions and conjugated aromatic linkers such as Cd(II) and aromatic polycarboxylate ligands may be promising candidates for potential photoactive materials.[26] In order to illustrate the fluorescence and confirm the effect of ligands on the fluorescence of **1**, we measured the maximum excitation (Fig. S3, ESI†) and emission spectra (Fig. 5) of the free acid $H_2$5-asba, the auxiliary ligand bimb and MOF **1**. The free acid $H_2$5-asba exhibits blue fluorescence with an emission maxima at 460 nm and a shoulder at

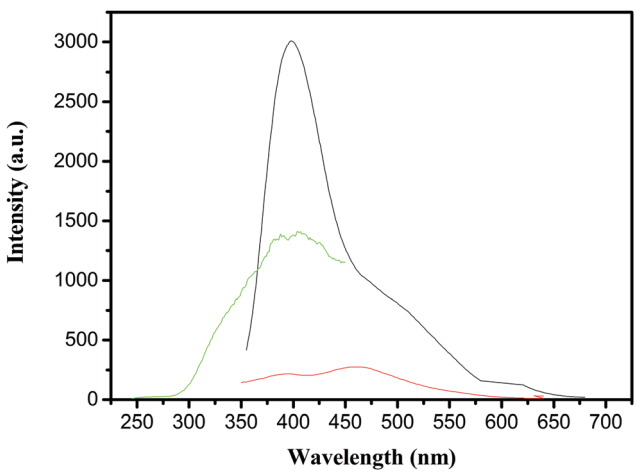

Fig. 5 The fluorescence emission spectra of $H_2$5-asba (red, λ_{ex} = 330 nm), bimb (green, λ_{ex} = 225 nm) and MOF **1** (black, λ_{ex} = 350 nm).

398 nm (λ_{ex} = 330 nm), and the emission peak of bimb is located at 400 nm (λ_{ex} = 225 nm). These emissions can be assigned to the π*–n transitions. MOF **1** exhibits one strong band with the maximum emission peak centered at *ca.* 399 nm (λ_{ex} = 350 nm), which is very similar to those of the auxiliary ligand bimb and the shoulder of $H_2$5-asba, indicating that the emission of MOF **1** may mainly be attributed to the intraligand π–π* transition further modified by Cd(II) coordination.[27] Compared with the maximum emission peak (460 nm) of $H_2$5-asba, **1** exhibits a significant blue-shifted fluorescence, indicating that metal-to-ligand charge transfer (MLCT) could also occur within the MOF.

The lowest excited singlet state S_1 of the free acid $H_2$5-asba and the auxiliary ligand bimb belongs to n–π* which is spin-forbidden. Accordingly, these ligands generate relatively weak fluorescence emissions. Once the ligands coordinate to Cd(II), the lowest excited singlet state S_1 converts into π–π* which is spin-permitted. Due to the enhanced effects of (1) the lowest excited singlet state S_1 from n–π* to π–π*, and (2) the ligation to the central Cd(II) ions which enhances the rigidity of the ligands and reduces the energy loss through a nonradiation pathway,[28] the emission intensity of MOF **1** is much stronger than the individual ligands.

Photoluminescence sensing behaviors

Sensing of solvent molecules. Based on the photoluminescent property of **1**, its photoluminescence sensing behaviors for some metal ions and NACs were analysed systematically. Usually, provided that MOFs are used as sensory materials, they should be dispersed in some organic solvents. To achieve a satisfactory analytic effect and make the results easier to distinguish, the material should have a relatively strong emission intensity in the selected solvent. Thus, the fluorescent properties of **1** were firstly investigated by dispersing a finely ground sample in 50 ml of various solvents (1.29 mg, 5×10^{-5} M) and sonicating for about three minutes. The emission intensities of **1** are highly dependent on the solvents: H_2O, ethanol, methanol, *N*,*N*-dimethylacetamide (DMA), dimethylsulfoxide (DMSO), *N*,*N*-diethylformamide (DEF) and *N*,*N*-dimethylformamide (DMF), *etc.* (Fig. 6). Clearly, acetone has the most significant quenching effect on the emission of the emulsion of **1**. Such solvent-dependent fluorescent properties are meaningful in the sensing of acetone, which is dangerous to human health and the environment. Interestingly, **1** possesses the strongest emission in water with a slightly red-shifted maximum peak located at 401 nm compared with that of the solid state emission, which may be due to the effect of water polarity on charge transfer.[29] Accordingly, in the following fluorescence sensing measurements, we selected water instead of organic solvent as the detection medium due to **1** having the strongest emission intensity as well as a high stability in water, which will not only make the measurements more close to the environmental aqueous condition but also make the results easier to understand merely from the changes of emission intensity, realizing the pleasing detection result. Thus, the well-ground sample **1** was dispersed in water to form a suspension in the following fluorescence detecting measurements, into which the corresponding solutions of analytes (metal ions and NACs) were added. The PXRD patterns of the sample **1** after immersion in all of the related solvents for about four days indicate that the host framework of **1** is quite stable in all of the solvents (Fig. 7).

Therefore, MOF **1** may be used as a potential good candidate for solvent-resistant photoluminescent materials due to its relatively strong fluorescence intensity, high framework thermal stability and insoluble feature in common solvents (Fig. 7).

Sensing of metal ions. To examine the potential of **1** for the sensing of metal ions (Na^+, K^+, Mg^{2+}, Ca^{2+}, Sr^{2+}, Ba^{2+}, Zn^{2+}, Cd^{2+}, Cu^{2+}, Ag^+, Mn^{2+}, Fe^{2+}, Co^{2+}, Ni^{2+}, Al^{3+}, Eu^{3+}, Tb^{3+}, Cr^{3+} and Fe^{3+}), we firstly determined the pH of aqueous suspensions of **1** (0.05 mM) containing different metal ions (0.075 mM) (Table S2, ESI†). Then, we carried out the pH stability of MOF **1** by measuring the PXRD patterns of the samples after immersion in the corresponding aqueous solutions of different metal

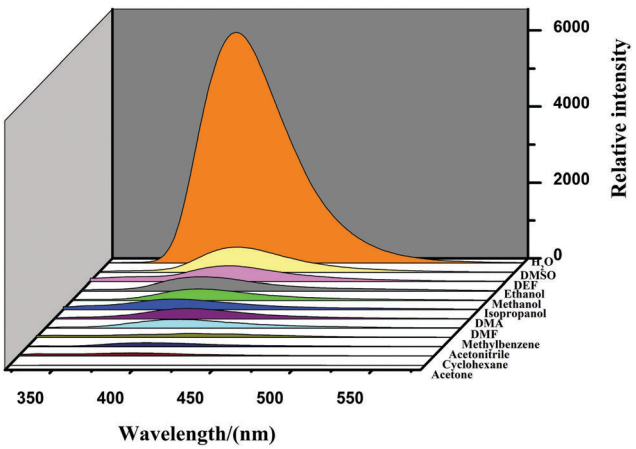

Fig. 6 The fluorescence spectra of **1** dispersed in various solvents.

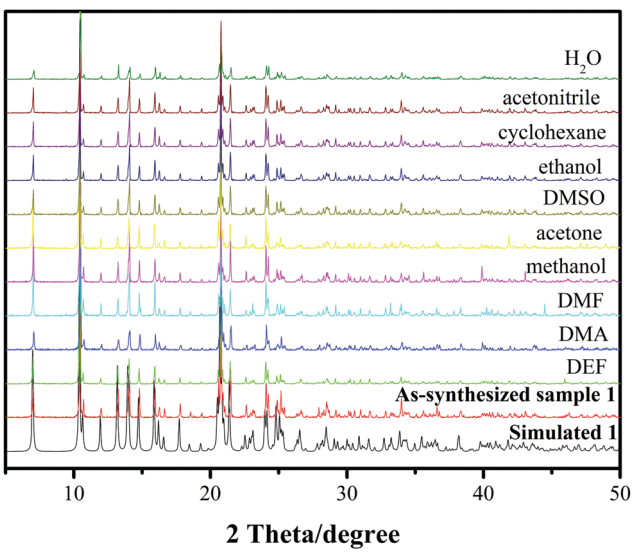

Fig. 7 The various PXRD patterns of the samples after immersion in different solvents for about four days, PXRD pattern of the bulk sample **1** and the simulated XRD pattern of **1** calculated from single-crystal X-ray data with Mercury 1.4.2.

ions (0.075 mM). The results indicate that MOF **1** shows high framework stability in all of the aqueous solutions of metal ions (Fig. S4, ESI†), including the aqueous Fe^{3+} solution with the lowest pH (4.26), which makes it possible for us to explore the sensing behavior for these metal ions in aqueous medium. Accordingly, an aqueous solution containing different metal ions (0.075 M, 2 μl) was added into the emulsions of **1** in water (2 ml cuvette with 1 cm width) and sonicated for about three minutes. The photoluminescence responses were recorded immediately (Fig. 8). As we can see, most of the metal ions have little effect on the fluorescence intensity of the suspensions of **1**. Specifically, the emission intensity of **1** at 400 nm decreases slightly when Al^{3+}, Cu^{2+}, Fe^{2+}, Tb^{3+}, Cr^{3+} and Eu^{3+} ions are added, but decreases significantly in the presence of Fe^{3+} ions [QP (quenching percentage) = $1 - I/I_0$ = 51.9%]. Here, I_0 is the initial fluorescence intensity without the analyte, and I is the fluorescence intensity after adding the analyte. This result indicates that **1** can sense Fe^{3+} ions efficiently through fluorescence quenching.[30,31]

MOF **1** shows the highest sensitivity for Fe^{3+} ions in comparison with other metal ions. This interesting behavior encourages us to further investigate the effects of the concentration of Fe^{3+} ions on the fluorescence intensities of the aqueous suspension of **1** in detail. The finely ground sample of **1** was dispersed in aqueous solution containing different concentrations of Fe^{3+} ions (0.01875–0.225 mM) to monitor the fluorescence response. The fluorescence titration experiment procedures are chiefly as follows: once the corresponding volumes of Fe^{3+} ions (0.075 M, from 0.5 μl to 6 μl) were added incrementally to the emulsion of the finely ground sample **1** in water (2 ml) and sonicated about three minutes, the fluorescence responses were immediately recorded. As is shown in Fig. 9, the fluorescence quenching is pronounced with a very low micromolar concentration of Fe^{3+} ions. With increasing the concentration of Fe^{3+} ions, the fluorescence emission was quenched continuously. It should be noted that a very low concentration of Fe^{3+} ions was good enough to show obvious detectable fluorescence quenching (0.01875 mM, 1 ppm, QP = 18.0%) of the fluorescence intensity of **1**. The quenching percentage reaches 83.3% when the concentration of

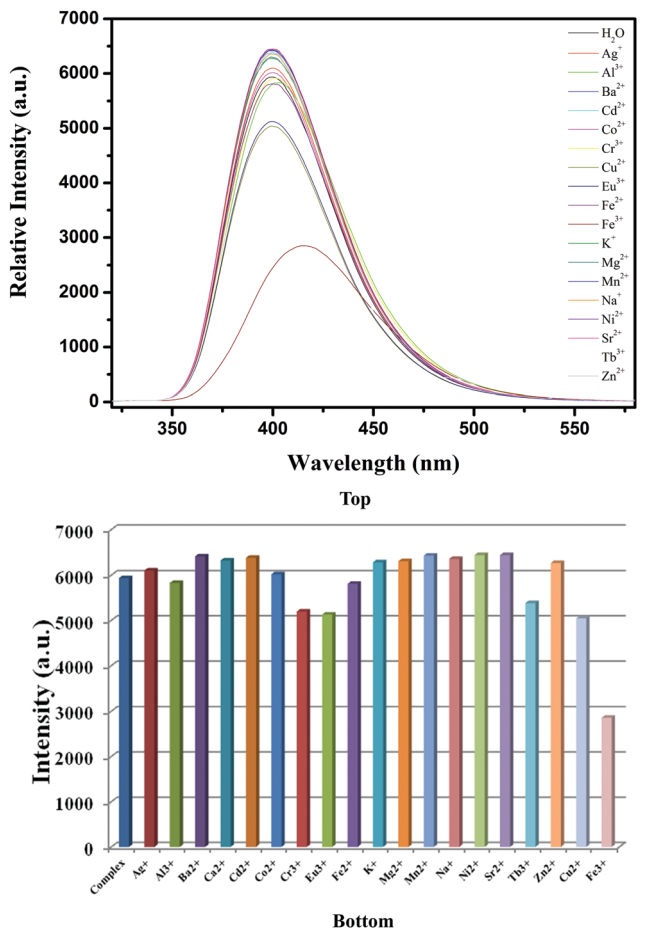

Fig. 8 (top) Fluorescence spectra of the emulsions of **1** by introducing different metal ions with the same concentration of 0.075 mM in the final mixture (λ_{ex} = 300 nm). (bottom) The relative maximum emission intensity corresponding to the different metal ions.

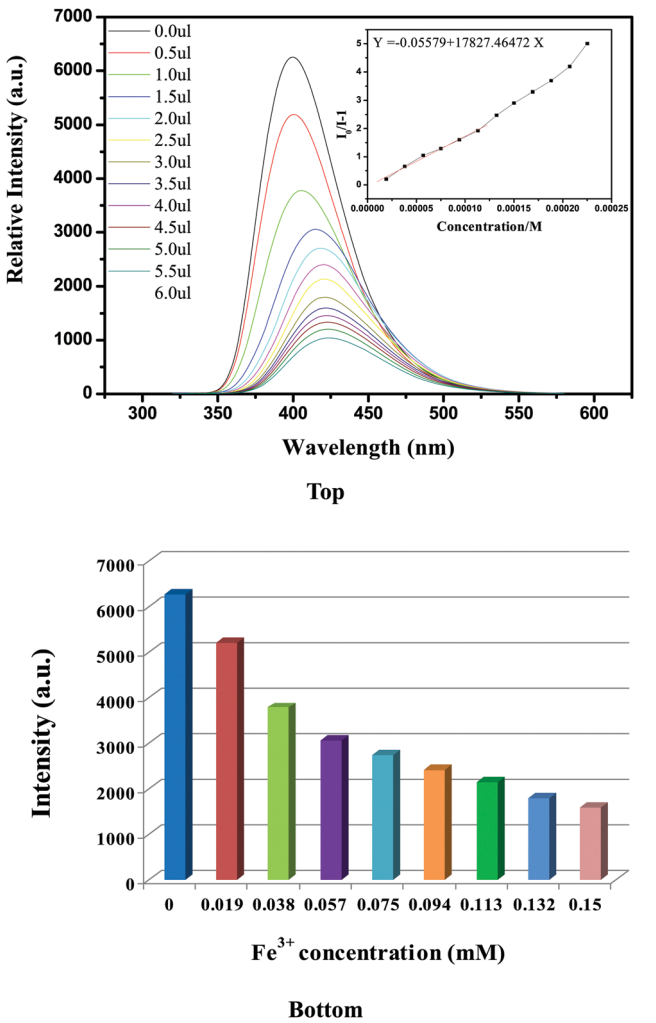

Fig. 9 Top: Fluorescence spectra of **1** dispersed in water (2 ml) with the incremental addition of Fe^{3+} aqueous solution (0.075 M). Inset: the best linear-fit of $I_0/I - 1$ *versus* [Fe^{3+}] in the low concentration. Bottom: The relative intensity of the maximum emissions corresponding to the different concentrations of Fe^{3+} ions (λ_{ex} = 300 nm).

Fe^{3+} ions in the emulsion is 0.225 mM, indicating that **1** shows rapid and high sensitivity for Fe^{3+} ions. The Stern–Volmer plots for Fe^{3+} ions are typically linear at low concentrations. To further reveal the quenching efficiency by Fe^{3+} ions, the fluorescence intensity *versus* [Fe^{3+}] plot at low concentration can be best linear-fitted into $I_0/I - 1 = K_{SV}[Fe^{3+}] - 0.05579$, which is very close to the Stern–Volmer equation $I_0/I - 1 = K_{SV}[A]$, where [A] is the molar concentration of the quencher, and K_{SV} is the Stern–Volmer quenching coefficient. The quenching coefficient K_{SV} for Fe^{3+} is estimated to be 1.78×10^4 L mol^{-1} for **1**, which is comparable to those well-designed solution-based organic compounds for the sensing of Fe^{3+} ions (K_{SV}: about 10^4 L mol^{-1}).[32]

In practical determination, it is quite usual that the detection aqueous media in the environment always contains some coexisting interfering metal ions. So, some common interfering metal ions, such as Na^+, Mn^{2+}, Tb^{3+}, Eu^{3+}, Ni^{2+}, Zn^{2+}, Cu^{2+}, Sr^{2+}, Co^{2+}, Fe^{2+}, Al^{3+}, Ag^+, Cr^{3+}, Ca^{2+}, Ba^{2+}, K^+, Mg^{2+} and Pb^{2+}, were included to test the fluorescence selective effect in order to generate simulative environmental conditions. Two pairs of contrast tests were thus designed for comparison: **1** + Fe^{3+} and **1** + interfering ions + Fe^{3+}. Keeping the concentration of Fe^{3+} ions at 0.075 mM in the emulsions of **1**, other interfering metal ions were then introduced to the emulsion system of **1** with the same concentration as that of the Fe^{3+} ions in the final mixture (0.075 mM). It is quite pleasing that the quenching effects by the Fe^{3+} ions on the fluorescence of the emulsion of **1** are almost not influenced by the interfering metal ions (Fig. 10), further confirming that **1** may act as a promising selective fluorescent sensor for Fe^{3+} ions in the environment.

To explore the potential of such a selective and sensitive Cd(II) MOF sensor for the detection of Fe^{3+} ions in a biological system, the finely ground sample of **1** was dispersed in a simulative physiological condition [20 mM 2-[4-(2-hydroxyethyl)-1-piperazinyl]ethanesulfonic acid (HEPES) aqueous buffer solution, pH = 7] with the incremental addition of Fe^{3+} ions. Fluorescence quenching titrations were then carried out on the suspension of **1**. It should be noted that the relative fluorescence intensity of the emulsion of **1** in HEPES aqueous buffer solution is similar to that in water, indicating that HEPES has almost no influence on the fluorescence intensity of the emulsion of **1** (Fig. 11). With increasing the concentration of Fe^{3+} ions, the fluorescence intensity of the emulsion of **1** decreased continuously, which is similar to that in aqueous solution. The quenching efficiency by Fe^{3+} ions under the simulative physiological conditions is higher than that in the aqueous suspension (0.075 mM Fe^{3+} in the HEPES buffer solution: QP = 61.1%). The emission of the suspension of **1** was quenched almost completely when the Fe^{3+} concentration was increased to 0.225 mM (QP = 94.07%). To further quantify the quenching efficiency by Fe^{3+} ions in the HEPES buffer solution, the relative photoluminescence intensity ($I_0/I - 1$) *versus* Fe^{3+} concentration is shown in Fig. 11. In low concentration, the intensity *versus* [Fe^{3+}] plot can also be best linear-fitted into

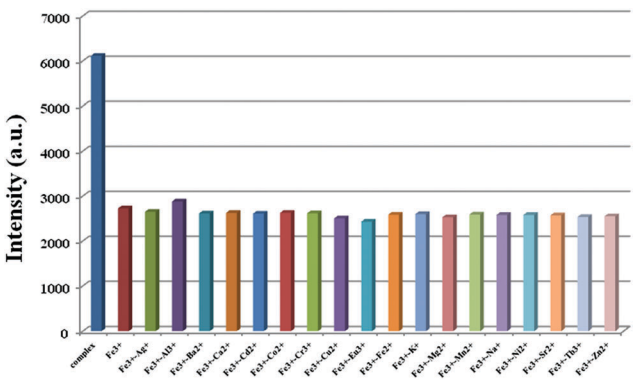

Fig. 10 The maximum emission intensity of **1**, showing the effects of the interfering metal ions on the interaction between **1** and Fe^{3+} ions in the dispersion. The concentration of Fe^{3+} ions and the interfering metal ions in the dispersion is 0.075 mM (λ_{ex} = 300 nm).

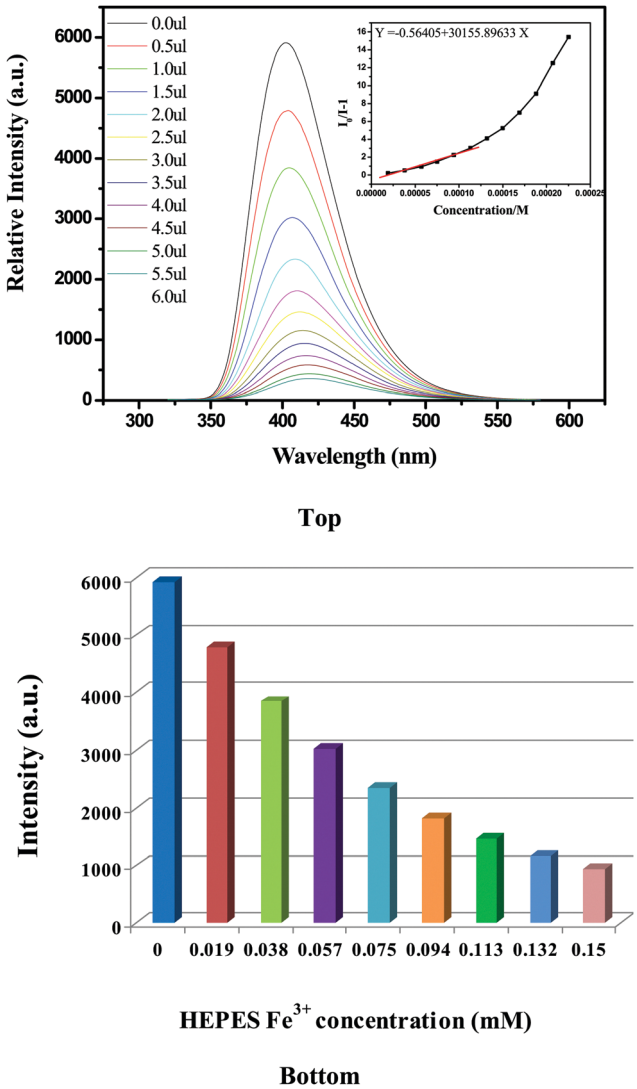

Fig. 11 Emission spectra and the best linear-fit of $I_0/I - 1$ *versus* [Fe^{3+}] in the low concentration (inset) (top) and maximum intensity (bottom) of **1** dispersed in HEPES aqueous buffer solution (pH = 7) upon incremental addition of an aqueous solution of Fe^{3+} ions (0.075 M) (λ_{ex} = 300 nm). The volumes of the water solution of Fe^{3+} ions added are indicated in the legend.

$I_0/I - 1 = 3.01 \times 10^4[Fe^{3+}] - 0.5645$ for **1**, which is also close to the Stern–Volmer equation $I_0/I - 1 = K_{SV}[A]$. In the simulative psychological conditions, the Stern–Volmer constant K_{SV} for Fe^{3+} ions is bigger than that in water, revealing **1** may also be used as an efficient fluorescent sensor for Fe^{3+} ions in a biological system.

In order to elucidate the fluorescence quenching mechanism of the suspension of **1** by Fe^{3+} ions, we further ran the PXRD measurements of the samples after immersion in the corresponding aqueous solution and HEPES aqueous buffer solution of Fe^{3+} ions (0.225 mM, pH = 3.48 for aqueous Fe^{3+} solution) for about five hours. Both the PXRD patterns are consistent with that of the as-synthesized sample of **1** (Fig. 12), suggesting that the original framework of **1** doesn't transform in the aqueous and the HEPES aqueous buffer solutions of Fe^{3+} ions and the central Cd(II) ions aren't exchanged with the analyte Fe^{3+} ions during the sensing process. The paramagnetic high-spin Fe^{3+} ion with d^5 configuration belongs to the "hard acid" type and has strong electron-withdrawing ability. So, during the sensing process, the Fe^{3+} ion can generate the strongest electrostatic interactions with the electron-rich sulfonate group of the ligand 5-asba^{2-} $[(-S_{sulfonate}O_3)^- \cdots Fe^{3+}]$ in the fluorophore compared with other metal ions, and consequently absorb more energy from the fluorophore, which makes the energy of fluorescence emission the smallest among all of the investigated metal ions, resulting in the obvious red-shifted emission. Chemists have reported that the possibility of resonance energy transfer depends greatly on the degree of spectral overlap between the emission spectrum of the fluorophore and the absorption spectrum of the analyte. The spectral overlap is the basic requirement for an energy transfer process. If there is no overlap, the quenching effect can be attributed to the electron transfer process.[12c,19a,29a,33] The overlap between the absorption spectrum of aqueous Fe^{3+} solution and the emission spectrum of the aqueous suspension of **1** (Fig. S5, ESI†) further confirms that the higher quenching effect by the high spin Fe^{3+} ions can be attributed to the energy transfer (ET) mechanism.[9d,e,34]

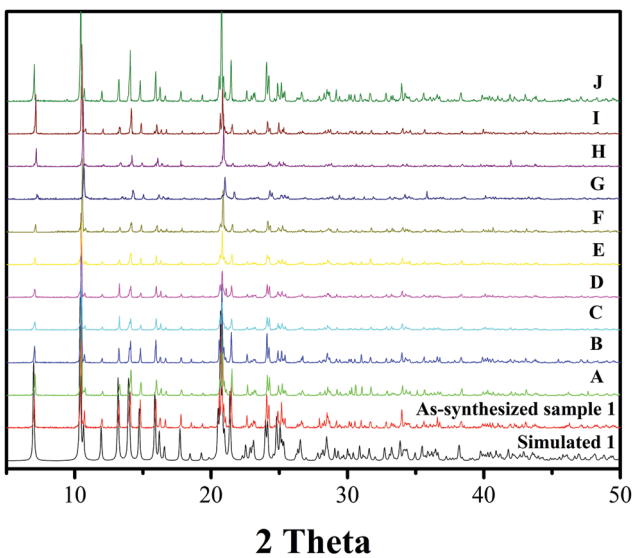

Fig. 12 The simulated XRD pattern of **1** calculated from single-crystal X-ray data with Mercury 1.4.2., the PXRD patterns of the as-synthesized sample **1** and the samples after immersion in 0.225 mM aqueous solution of Fe^{3+} ions (A), HEPES aqueous buffer solution containing 0.225 mM Fe^{3+} ions (B), 0.225 mM aqueous–methanol solution of 4-NP (C), 4-NA (D), 2-M-4-NA (E), NB (F), 2-NP (G), 3-NP (H), 3-M-2-NP (I) and 1.3-DNB (J).

In summary, the Stern–Volmer constants in both environmental and simulative psychological conditions are comparable with those of the reported novel MOF-based sensory materials and well-designed solution-based organic compounds for the sensing of Fe^{3+} ions,[9d,e,32,34] indicating the potential use of **1** for efficient and selective detection of trace amounts of Fe^{3+} ions in both environmental and biological systems.

Sensing of aromatic compounds. As mentioned above, rapid and efficient detection of industry pollutants in aqueous media, such as benzene compounds, especially for nitroaromatic compounds (NACs), is very important. Therefore, different benzene compounds in methanol solution (0.075 M, from 0.5 μl to 6 μl) were added incrementally into the aqueous suspensions of **1** (2 ml) to determine its sensing behaviors toward these aromatic compounds. It should be noted that the volume of methanol solution added can be neglected in the final mixture because the maximum volume is only 6 μl (from 0.5 μl to 6 μl), which is too small compared with that of the aqueous suspension (2 ml) detected. We first selected some general aromatic compounds, such as benzene (BZ), toluene (TO), chlorobenzene (CB), phenol (PL) and nitrobenzene (NB) as the analytes. The results show that only electron-deficient nitrobenzene can quench the emission of the suspension of **1** with a quenching percentage (QP) of about 50% when the concentration of NB is 0.075 mM (Fig. 13 and Fig. S6, ESI†). Furthermore, the emission intensity *vs.* [NB] plot in low concentration can be best linear-fitted into $I_0/I - 1 = K_{SV}[NB] - 0.17612$, which is very close to the Stern–Volmer equation $I_0/I - 1 = K_{SV}[A]$ (Fig. 14). The quenching coefficient K_{SV} (1.6×10^4 L mol^{-1}) is comparable to those well-designed novel MOFs for the sensing of NB.[19a,29a,35]

To study the quenching mechanism of NB, we firstly recorded the PXRD pattern of the sample after immersion in 0.225 mM NB aqueous solution for five hours. The result

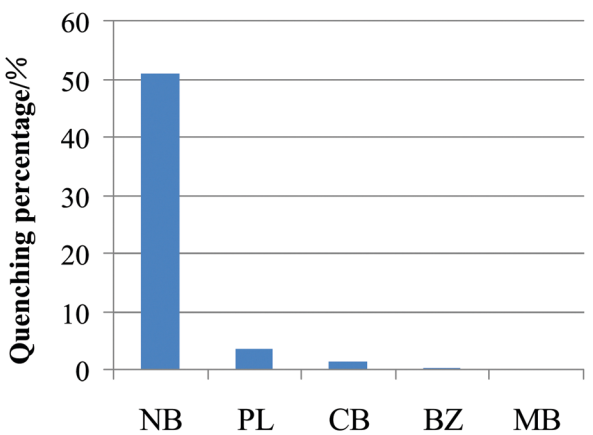

Fig. 13 Quenching percentage of fluorescence obtained for introducing different benzene compounds (0.075 mM) into the aqueous emulsions of **1**.

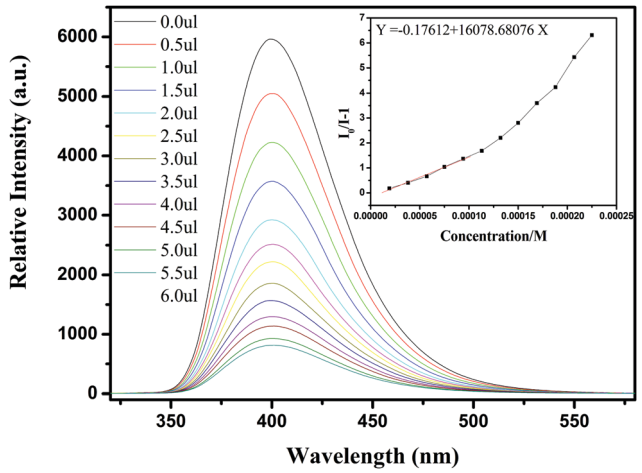

Fig. 14 Fluorescence spectra of **1** dispersed in water with incremental addition of NB in methanol (0.075 M). The volumes of methanol solution of NB added are indicated in the legend. Inset: the best linear-fit of $I_0/I - 1$ *versus* [Fe^{3+}] in the low concentration.

indicates that the framework keeps its integrity in aqueous NB solution (Fig. 12). Owing to the absence of porosity in the MOF, the incorporation of NB molecules into the channels of **1** is impossible, but the finely ground MOF particles could be dispersed well in the aqueous suspension, which makes it possible for the NB molecules to be adsorbed tightly on the surface of the MOF particles and enables the possibility of excited MOF–NB close contact. Fig. 15 shows that the absorption spectrum of the aqueous NB solution has almost no overlap with the emission spectrum of the suspension of **1**. So, the fluorescence quenching mechanism can be ascribed to the photo-induced electron transfer (PET) from the electron-rich excited MOF to the electron-deficient NB molecules.[8a,16b,17,36]

This interesting result encourages us to further explore the sensing potential of **1** for other NACs. Thus, various analogues such as 1,3-dinitrobenzene (1,3-DNB), 3-methyl-2-nitrophenol (3-M-2-NP), 4-nitrophenol (4-NP), 3-nitrophenol (3-NP), 2-nitrophenol (2-NP), 4-nitroaniline (4-NA) and 2-methyl-4-nitroaniline (2-M-4-NA) were used as the investigated reagents. The basic framework of **1** keeps high stability in all of the corresponding aqueous solutions of NACs (Fig. 12), which makes it possible for us to explore the sensing behaviors of the MOF for these NACs in aqueous medium. Similar to the method of studying the sensing property for NB, the methanol solutions of the corresponding NACs (0.075 M) were gradually added into the aqueous suspensions of **1** (2 ml) and sonicated for about three minutes, then the fluorescence responses were immediately recorded by photoluminescence spectroscopy. The results show that all NACs can weaken the fluorescence intensity of the suspension of **1**, but the quenching percentage exhibits a big difference. Fig. 16 shows the fluorescence quenching percentage (QP) when the concentration of the corresponding NACs is 0.075 mM in the aqueous suspension. The addition of 3-NP, 3-M-2-NP, NB and 1,3-DNB solution caused relatively little fluorescence intensity change of the suspension, but the introduction of nitroaniline homologues (4-NA and 2-M-4-NA) produced significant quenching of the fluorescence intensity (0.075 mM, QP: 88.01 for 4-NA and 86.70% for 2-M-4-NA, respectively). It can be seen from Fig. 17 that the fluorescence quenching by 4-NA and 2-M-4-NA could be detected at a very low concentration (3.75 μM: 0.52 ppm for 4-NA and 0.68 ppm for 2-M-4-NA), indicating the extremely high sensitivity towards 4-NA and 2-M-4-NA. The fluorescence intensity decreased continuously upon incremental addition of the corresponding methanol solution of 4-NA and 2-M-4-NA into a standard aqueous emulsion of **1**, and the Cd(II)-centered emission was almost completely quenched when the concentration of 4-NA and 2-M-4-NA in the suspension finally reached 0.225 mM (QP: 98.99% for 4-NA and 97.65% for 2-M-4-NA). The intensity *versus* [NACs] in the low concentration can all be best linear-fitted into $I_0/I - 1 = K_{SV}[A] + b$, which are all close to the Stern–Volmer (SV) equation, $I_0/I - 1 = K_{SV}[A]$ (Fig. 17 and Fig. S7, ESI†). According to the calculation, the Stern–Volmer constants for the NACs were found to be in the following order: 4-NA > 2-M-4-NA > 4-NP > 2-NP > NB > 3-NP > 3-M-2-NP > 1,3-DNB (Table 3, Table S1, ESI† and Fig. 18), further confirming that **1** can be used as an efficient multi-responsive fluorescent sensor for the detection of trace amounts of some NACs, especially for

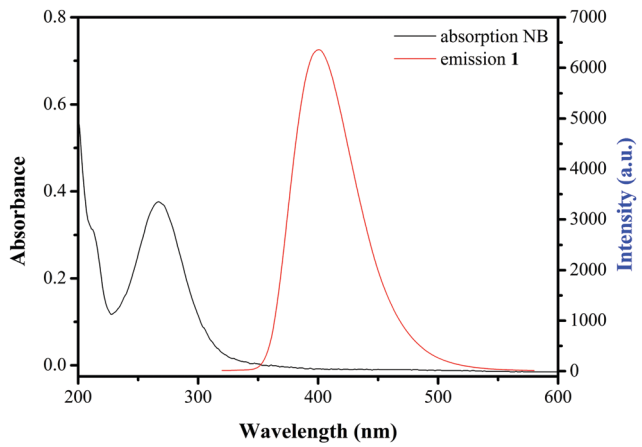

Fig. 15 The absorption spectrum of NB and the emission spectrum of **1** in aqueous medium.

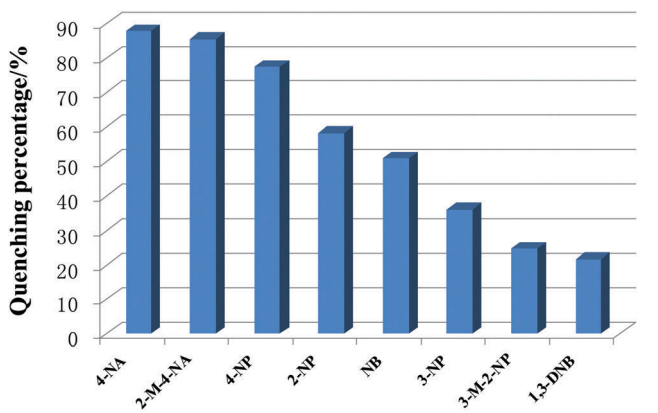

Fig. 16 Percentage of fluorescence quenching obtained by introducing different NACs (0.075 mM) into the emulsion of **1**.

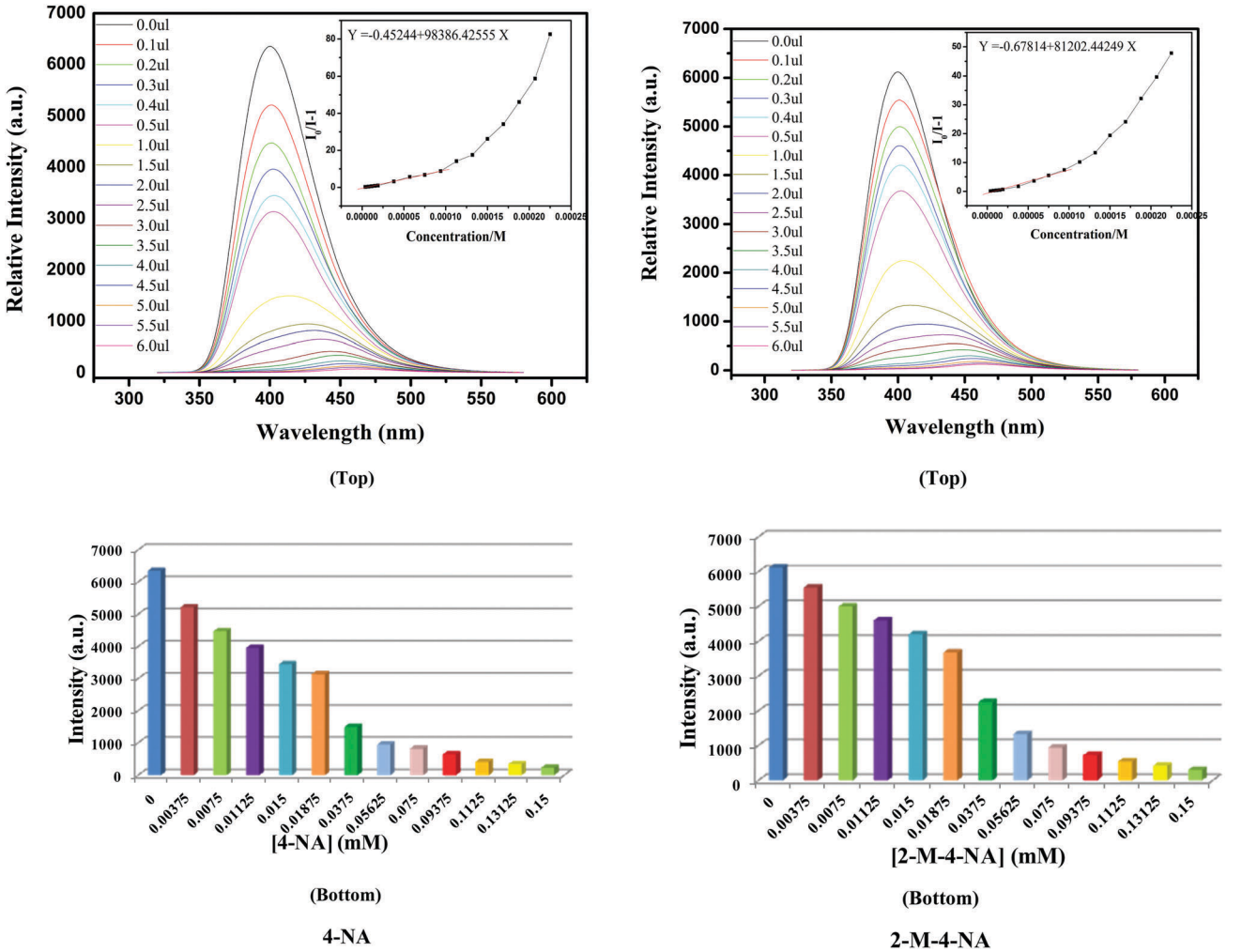

Fig. 17 Photoluminescence spectra and the best linear fit of $I_0/I - 1$ *versus* concentration (inset) (top), the relative intensity of the maximum emission *versus* concentration (bottom) of **1** dispersed in water with the incremental addition of corresponding 4-NA and 2-M-4-NA in methanol.

Table 3 Selected Stern–Volmer constants (K_{SV}) for some NACs

NACs	K_{SV} (L mol^{-1})	NACs	K_{SV} (L mol^{-1})
4-NA	9.8×10^4	2-M-4-NA	8.1×10^4
NB	1.6×10^4		

4-NA and 2-M-4-NA (K_{SV} = 9.8×10^4 L mol^{-1} and 8.1×10^4 L mol^{-1}, respectively). The Stern–Volmer constants K_{SV} for 2-M-4-NA and 3-M-2-NP are smaller than those of the corresponding 4-NA and 2-NP, indicating that the electron donating group –methyl in 4-NA and 2-NP can decrease the quenching efficiency.

To our best knowledge, **1** is the first MOF that can be used as a potential efficient sensor for 4-NA and 2-M-4-NA simultaneously.

Due to the absence of void space within the MOF, the sensing mechanism might be quite different from most cases of guest-induced quenching, in which the quencher molecules penetrate into the MOF channels and interact with the host framework, resulting in a photoluminescence response. Therefore, we proposed that surface-based interactions are the main cause of quenching for this MOF. The most efficient sensitivity of **1** for 4-NA and 2-M-4-NA is due to the nitro group in the 4-position of the aromatic ring having a strong electron-withdrawing and conjugate effect, which can make 4-NA and 2-M-4-NA interact strongly with the fluorophore *via* the collisional encounters between the π conjugated moieties of the electron-rich organic ligands in the excited MOF and the electron-deficient analytes (4-NA and 2-M-4-NA) as well as the hydrogen bonds between the multifunctional groups (carboxylate/sulfonate/amino) of 5-asba^{2-} and amino/nitro groups of 4-NA and 2-M-4-NA. So, the efficient fluorescence quenching of **1** by 4-NA and 2-M-4-NA can be maintained over a long range due to strong electrostatic interactions and the energy transfer from the fluorophore to the analytes (4-NA and 2-M-4-NA),[12c,19a,29a,33] which was confirmed by the very large overlap between the absorption spectra of 4-NA and 2-M-4-NA and the emission spectrum of **1** in aqueous medium (Fig. S8, ESI†).

In Fig. 17, with the increase in concentration of 4-NA and 2-M-4-NA, there were two peaks in the emission of the MOFs: one red-shifted peak around 450 nm and one shoulder at about 400 nm. In order to investigate the origin of these two peaks,

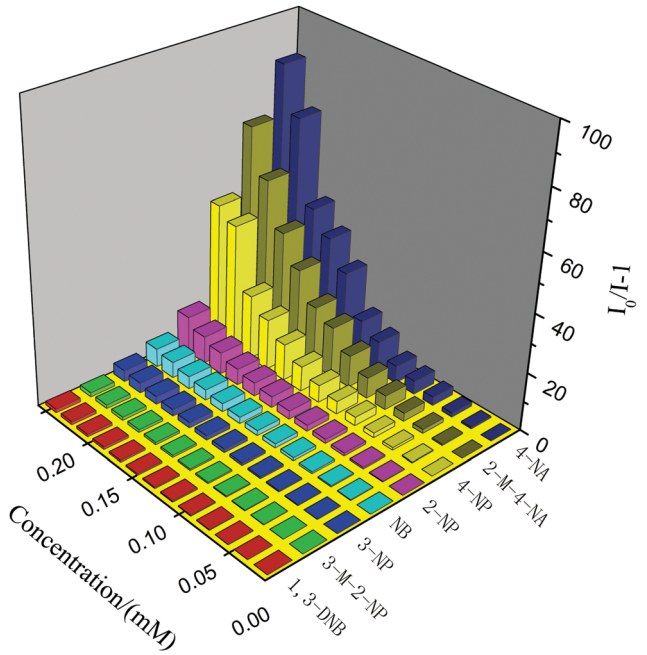

Fig. 18 Corresponding ($I_0/I - 1$) *versus* concentration plots of the analytes for **1**.

we firstly recorded the fluorescence emission spectra of the aqueous solutions of 4-NA and 2-M-4-NA by incrementally adding methanol solution of 4-NA and 2-M-4-NA (0.075 M) into 2 ml of water, respectively. The results indicate that there are almost no fluorescence responses for aqueous solutions of 4-NA and 2-M-4-NA (Fig. S9, ESI†). Considering that interactions such as hydrogen bonding and electrostatic interactions exist between the excited MOF and analytes, *e.g.*, $-SO_3$-(MOF)/$-NH_2$(4-NA) and $-NH_2$(MOF)/$-NO_2$(4-NA), these two emissions could be attributed to the multi-recognition capability of the MOF. We think that the two emissions shall correspond to two types of the supramolecular "pair". When the concentration of the analyte (4-NA or 2-M-4-NA) molecules is low, the system firstly formed the supramolecular "pair" *via* interactions, *e.g.*, hydrogen bonding and electrostatic interactions, occupying partial recognition sites on the excited MOF. Once the first recognition sites were saturated, the remaining sites began to recognize the analyte molecules, leading to another type of supramolecular "pair". The more the recognition sites on the excited MOF are occupied by the quencher molecules, the more energy will be absorbed. Consequently, the residue of the firstly-formed "pairs" corresponded to the shoulder, while the later-formed "pairs" to the red-shifted peak.

It should be noted that, compared with 4-NP, 2-NP and 3-NP have relatively less fluorescence quenching effect on the fluorescence intensity of the emulsion of **1** (0.075 mM, QP: 58.41 by 2-NP; 35.83 by 3-NP; 77.18% by 4-NP). The order of the fluorescence quenching coefficients K_{SV} for the nitrophenol isomers in the aqueous emulsions of **1**: 4-NP > 2-NP > 3-NP further indicates that **1** can discriminate the nitrophenol isomers efficiently. To our best knowledge, this is the first MOF that can be used to discriminate nitrophenol isomers efficiently through fluorescence sensing. The Stern–Volmer constant K_{SV} (6.1×10^4 L mol^{-1}) for 4-NP is comparable with those of the reported MOFs as efficient fluorescence sensors for 4-NP,[37] indicating that **1** can also be used to detect 4-NP selectively among the three nitrophenol isomers (2-, 3-, 4-NP), which is possible due to the –OH group of 4-NP having the highest acidity among three isomers. Thus, the highest acidic –OH group of 4-NP deprotonates relatively easily into anions, which can generate the strongest long range electrostatic interactions with the fluorophore, leading to the efficient energy transfer from the excited MOF to 4-NP. This is also confirmed by the relatively large overlap between the absorption band of aqueous solution of 4-NP and the emission band of the emulsion of MOF (Fig. S10, ESI†). So, the quenching mechanism is very similar to that of the nitroaniline homologues (4-NA and 2-M-4-NA).[12c,19a,29a,33]

Experimental section

Materials and characterization

The auxiliary flexible nitrogenous ligand 1,4-bis(1*H*-imidazol-1-yl)-butane (bimb), was synthesized according to the documented method.[38] The other reagents were obtained commercially.

FT-IR spectra (400–4000 cm^{-1}) were recorded from a KBr pellet in a Magna 750 FT-IR spectrophotometer. The fluorescence spectra were recorded using an F-4500 Fluorescence spectrophotometer (Hitachi). Both the excitation and emission pass width were 5.0 nm. Solid state diffuse reflectance UV-vis spectra were collected on a finely ground powder sample with a Cary 5000 spectrophotometer. Diffuse reflectivity was determined from 200 to 800 nm using $BaSO_4$ as a standard with 100% reflectance. The UV-vis absorption spectra of aqueous solution (5.63×10^{-5} M) were recorded on a UV-2501PC (Hitachi) spectrophotometer. Thermogravimetric analysis (TGA) was run on a NETZSCH STA 409 PG/PC instrument from room temperature to 800 °C at a heating rate of 10 °C min^{-1} in N_2. The determination of pH was carried out with a LeiCi PHS-25 acidometer. Powder X-ray diffraction data (PXRD) were collected on a computer-controlled Bruker D8 Advanced XRD diffractometer equipped with a Cu-K_α monochromator (λ = 1.5418 Å) at a scanning rate of 0.02° s^{-1} from 5° to 50°.

Synthesis of {[Cd(5-asba)(bimb)]}$_n$ (1)

A mixture containing $CdCl_2 \cdot 2.5H_2O$ (0.034 g, 0.150 mmol), $H_2$5-asba (0.0326 g, 0.150 mmol), bimb (0.029 g, 0.150 mmol), NaOH (0.006 g, 0.150 mmol) and H_2O (8 ml) was sealed in a Teflon reactor, which was heated at 120 °C for three days, before it was cooled to room temperature at 10 °C h^{-1}. Block crystals were collected in a 65% yield. Anal. calc. for $C_{17}H_{19}CdN_5O_5S$: C, 34.43; H, 3.69; N, 13.52. Found: C, 34.34; H, 3.60; N, 13.43%. IR/cm^{-1} (KBr): 3301 (s), 3233 (s), 3178 (s), 3137 (s), 2936 (w), 1611 (vs), 1535 (vs), 1433 (s), 1371(s), 1255 (s), 1180 (s), 1090 (s), 1022 (s), 954 (s), 892 (s), 817 (m), 755 (m), 673 (s), 584 (s).

The phase purity of **1** was further verified by the PXRD pattern of the bulk sample which is consistent with the

corresponding simulated one calculated from single crystal X-ray diffraction data with Mercury 1.4.2 (Fig. 7).[39]

Single-crystal X-ray structure determination

Crystallographic data for **1** were collected at 293(2) K with a Siemens SMART CCD diffractometer using graphite-monochromated (Mo/K_α) radiation (λ = 0.71073 Å), ψ and ω scans mode. The structure was solved by direct methods and refined by full-matrix least-squares on the $|F|^2$ method. Intensity data were corrected for Lorenz and polarization effects and a multi-scan absorption correction was performed. All non-hydrogen atoms were refined anisotropically. The carbon/nitrogen-bound H atoms of **1** were added geometrically and allowed to ride on their respective parent atoms. The contribution of these hydrogen atoms was included in the structure factor calculations. All calculations were carried out using the SHELXL-97 program.[40] Crystallographic data and experimental details for **1** are given in Table 1.

Fluorescence sensing study

Sensing of solvents. Finely ground samples of **1** (1.29 mg) were dispersed in 50 ml of solvents: H_2O, methanol, ethanol, acetone, acetonitrile, cyclohexane, DMSO, DEF, DMA and DMF (5×10^{-5} M). The emulsion was placed in a 2 ml cuvette with 1 cm width and then sonicated for about three minutes. The fluorescence emission spectra were recorded immediately.

Sensing of aromatic compounds. Methanol solutions of the corresponding aromatic compounds (0.075 M) were added incrementally into the aqueous emulsions of **1** (2 ml, 5×10^{-5} M) and sonicated for about three minutes. The fluorescence responses were then measured at once.

Sensing of metal ions. The same procedures as those for sensing the aromatic compounds were followed, except that the methanol solutions of aromatic compounds were replaced by aqueous solutions of $(NH_4)_2Fe(SO_4)_2{\cdot}6H_2O$ and $M(NO_3)_x$ (M^{n+} = Na^+, K^+, Mg^{2+}, Ca^{2+}, Sr^{2+}, Ba^{2+}, Zn^{2+}, Cd^{2+}, Cu^{2+}, Ag^+, Mn^{2+}, Co^{2+}, Ni^{2+}, Al^{3+}, Eu^{3+}, Tb^{3+}, Cr^{3+} and Fe^{3+}).

Study in the simulative physiological conditions. Based on the literature method,[41] 2-[4-(2-hydroxyethyl)-1-piperazinyl]ethanesulfonic acid (HEPES) was used as the reagent to create the simulative physiological conditions. HEPES aqueous buffer solution (20 mM, pH = 7) was prepared by adding 238 mg of HEPES into 50 ml of water. Then, the finely ground sample of **1** (1.29 mg) was dispersed into 50 ml of HEPES aqueous buffer solution (5×10^{-5} M).

Conclusions

In summary, a novel Cd(II)–organic framework **1** based on the multi-functional ligand $H_2$5-asba with α-Po topology has been successfully prepared, which exhibits excellent photoluminescence properties with solvent-dependent fluorescence intensities, and the strongest emission is observed in water. MOF **1** can rapidly and selectively sense Fe^{3+} ions in environmental and biological systems at about a one ppm level. The most striking property of **1** is its rapid and efficient detection for trace amounts of some NACs in aqueous medium, especially for nitroaniline homologues (4-NA and 2-M-4-NA), which makes it a promising potential fluorescent sensor simultaneously for these NACs. The systematic study reveals that **1** shows better fluorescence sensing towards nitroaniline homologues (4-NA and 2-M-4-NA) than other electron-deficient aromatics. To our best knowledge, **1** is the first example of a MOF-based fluorescent probe for 4-NA and 2-M-4-NA. Furthermore, **1** can discriminate the nitrophenol isomers (2-, 3- and 4-NP) efficiently through fluorescence sensing. In short, **1** is a novel MOF-based sensor with multi-responsive fluorescence sensing properties. Further studies will focus on the construction of other photoluminescent MOFs based on the multifunctional ligand $H_2$5-asba and their potential application in the detection of environmental chemical pollutants.

Acknowledgements

We gratefully acknowledge the Natural Science Foundation of Jiangsu Province (BK2012680), the Analysis and Testing Center of Yangzhou University, the Priority Academic Program Development of Jiangsu Higher Education Institutions (PAPD), and the Top-notch Academic Programs Project of Jiangsu Higher Education Institutions (PPZY2015B112).

References

1 (*a*) N. C. Andrews, *N. Engl. J. Med.*, 1999, **341**, 1986; (*b*) J. D. Haas and T. Brownlie, *J. Nutr.*, 2001, **131**, 676S.
2 V. A. Elrod, K. S. Johnson and K. H. Coale, *Anal. Chem.*, 1991, **63**, 893.
3 Z. O. Tesfaldet, J. F. van Staden and R. I. Stefan, *Talanta*, 2004, **64**, 1189.
4 K. Akatsuka, J. W. McLaren, J. W. Lam and S. S. Berman, *J. Anal. At. Spectrom.*, 1992, **7**, 889.
5 A. Ohashi, H. Ito, C. Kanai, H. Imura and K. Ohashi, *Talanta*, 2005, **65**, 525.
6 (*a*) M. M. Wanderley, C. Wang, C.-D. Wu and W. Lin, *J. Am. Chem. Soc.*, 2012, **134**, 9050; (*b*) Y. Guo, X. Feng, T. Han, S. Wang, Z. Lin, Y. Dong and B. Wang, *J. Am. Chem. Soc.*, 2014, **136**, 15485; (*c*) Z.-Z. Lu, R. Zhang, Y.-Z. Li, Z.-J. Guo and H.-G. Zheng, *J. Am. Chem. Soc.*, 2011, **133**, 4172; (*d*) N. B. Shustova, A. F. Cozzolino, S. Reineke, M. Baldo and M. Dinca, *J. Am. Chem. Soc.*, 2013, **135**, 13326.
7 (*a*) Z.-B. Han, Z.-Z. Xiao, M. Hao, D.-Q. Yuan, L. Liu, N. Wei, H.-M. Yao and M. Zhou, *Cryst. Growth Des.*, 2015, **15**, 531; (*b*) J.-S. Qin, S.-R. Zhang, D.-Y. Du, P. Shen, S.-J. Bao, Y.-Q. Lan and Z.-M. Su, *Chem. – Eur. J.*, 2014, **20**, 5625; (*c*) C.-X. Yang, H.-B. Ren and X.-P. Yan, *Anal. Chem.*, 2013, **85**, 441; (*d*) K. Jayaramulu, R. P. Narayanan, S. J. George and T. K. Maji, *Inorg. Chem.*, 2012, **51**, 10089; (*e*) J. Cao, Y. Gao, Y. Wang, C. Du and Z. Liu, *Chem. Commun.*, 2013, **49**, 6897; (*f*) S. Bhattacharyya, A. Chakraborty, K. Jayaramulu, A. Hazra and T. K. Maji, *Chem. Commun.*, 2014, **50**, 13567;

(*g*) J.-M. Zhou, W. Shi, H.-M. Li, H. Li and P. Cheng, *J. Phys. Chem. C*, 2014, **118**, 416; (*h*) B. Chen, L. Wang, Y. Xiao, F. R. Fronczek, M. Xue, Y. Cui and G. Qian, *Angew. Chem., Int. Ed.*, 2009, **48**, 500.

8 (*a*) S. Pramanik, C. Zheng, X. Zhang, T. J. Emge and J. Li, *J. Am. Chem. Soc.*, 2011, **133**, 4153; (*b*) Z. Hu, B. J. Deibert and J. Li, *Chem. Soc. Rev.*, 2014, **43**, 5815; (*c*) D. K. Singha, S. Bhattacharya, P. Majee, S. K. Mondal, M. Kumar and P. Mahata, *J. Mater. Chem. A*, 2014, **2**, 20908.

9 (*a*) P. Wang, J. P. Ma and Y. B. Dong, *Chem. – Eur. J.*, 2009, **15**, 10432; (*b*) G. G. Hou, Y. Liu, Q. K. Liu and Y. B. Dong, *Chem. Commun.*, 2011, **47**, 10731; (*c*) S. Dang, E. Ma, Z.-M. Sun and H. Zhang, *J. Mater. Chem.*, 2012, **22**, 16920; (*d*) M. Zheng, H. Tan, Z. Xie, L. Zhang, X. Jing and Z. Sun, *ACS Appl. Mater. Interfaces*, 2013, **5**, 1078; (*e*) X.-Y. Xu and B. Yan, *ACS Appl. Mater. Interfaces*, 2015, **7**, 721; (*f*) Z. Xiang, C. Fang, S. Leng and D. Cao, *J. Mater. Chem. A*, 2014, **2**, 7662; (*g*) J.-N. Hao and B. Yan, *J. Mater. Chem. C*, 2014, **2**, 6758; (*h*) Q. Tang, S. Liu, Y. Liu, J. Miao, S. Li, L. Zhang, Z. Shi and Z. Zheng, *Inorg. Chem.*, 2013, **52**, 2799; (*i*) Z. Chen, Y. Sun, L. Zhang, D. Sun, F. Liu, Q. Meng, R. Wang and D. Sun, *Chem. Commun.*, 2013, **49**, 11557.

10 Y. Salinas, R. Martinez-Manez, M. D. Marcos, F. Sancenon, A. M. Castero, M. Parra and S. Gil, *Chem. Soc. Rev.*, 2012, **41**, 1261.

11 (*a*) M. Kandpal, A. K. Bandela, V. K. Hinge, V. R. Rao and C. P. Rao, *ACS Appl. Mater. Interfaces*, 2013, **5**, 13448; (*b*) B. Zu, Y. Guo and X. Dou, *Nanoscale*, 2013, **5**, 10693; (*c*) J. M. Sylvia, J. A. Janni, J. Klein and K. M. Spencer, *Anal. Chem.*, 2000, **72**, 5834.

12 (*a*) A. Rose, Z. Zhu, C. F. Madigan, T. M. Swager and V. Bulovic, *Nature*, 2005, **434**, 876; (*b*) S. W. Thomas, G. D. Joly and T. M. Swager, *Chem. Rev.*, 2007, **107**, 1339; (*c*) Y. Peng, A. J. Zhang, M. Dong and Y. W. Wang, *Chem. Commun.*, 2011, **47**, 4505.

13 (*a*) S. Liu, Z. Xiang and D. Cao, *J. Mater. Chem.*, 2011, **21**, 6649; (*b*) T. Naddo, Y. Che, W. Zhang, K. Balakrishnan, X. Yang, M. Yen, J. Zhao, J. S. Moore and L. Zang, *J. Am. Chem. Soc.*, 2007, **129**, 6978; (*c*) S. Shaligram, P. P. Wadgaonkar and U. K. Kharul, *J. Mater. Chem.*, 2014, **2**, 13983; (*d*) S. Ghosh and P. S. Mukherjee, *Organometallics*, 2008, **27**, 316; (*e*) G. V. Zyryanov, M. A. Palacios and P. Anzenbacher, *Org. Lett.*, 2008, **10**, 3681; (*f*) B. Gole, S. Shanmugamraju, A. K. Bar and P. S. Mukherjee, *Chem. Commun.*, 2011, **47**, 10046; (*g*) B. Gole, A. K. Bar and P. S. Mukherjee, *Chem. Commun.*, 2011, **47**, 12137.

14 (*a*) E. Wang, D. Sun, H. Li, X. Sun, J. Liu, Z. Ren and S. Yan, *J. Mater. Chem. C*, 2016, **4**, 6756; (*b*) D. D. Li, J. Z. Liu, R. T. K. Kwok, Z. Q. Liang, B. Z. Tang and J. H. Yu, *Chem. Commun.*, 2012, **48**, 7167; (*c*) Y. Wang, A. La, Y. Ding, Y. X. Liu and Y. Lei, *Adv. Funct. Mater.*, 2012, **22**, 3547; (*d*) Y. Tao, G. T. Li and H. S. Zhu, *J. Mater. Chem.*, 2006, **16**, 4521.

15 (*a*) L. Liu and S. G. Telfer, *J. Am. Chem. Soc.*, 2015, **137**, 3901; (*b*) R. Haldar, R. Matsuda, S. Kitagawa, S. J. George and T. K. Maji, *Angew. Chem., Int. Ed.*, 2014, **53**, 11772; (*c*) D. Dutta, A. G. Wong-Foy, D. W. Gidley and A. J. Matzger, *J. Am. Chem. Soc.*, 2015, **137**, 2651; (*d*) M. Zhang, G. X. Feng, Z. G. Song, Y. P. Zhou, H. Y. Chao, D. Q. Yuan, T. Y. Tan, Z. G. Guo, Z. G. Hu, B. Z. Tang, B. Liu and D. Zhao, *J. Am. Chem. Soc.*, 2014, **136**, 7241; (*e*) V. Benoit, R. Pillai, A. Orsi, P. Normand, H. Jobic, F. Nouar, P. Billemont, E. Bloch, S. Bourrelly, T. Devic, P. A. Wright, G. de Weireld, C. Serre, G. Maurin and P. L. Llewellyn, *J. Mater. Chem. A*, 2016, **4**, 1383; (*f*) H. C. Zhou, J. R. Long and O. M. Yaghi, *Chem. Rev.*, 2012, **112**, 673; (*g*) L. Ni, D. Liang, Y. Cai, G. Diao and Z. Zhou, *Dalton Trans.*, 2016, **45**, 7581.

16 (*a*) Y. J. Cui, Y. F. Yue, G. D. Qian and B. L. Chen, *Chem. Rev.*, 2012, **112**, 1126; (*b*) L. E. Kreno, K. Leong, O. K. Farha, M. Allendorf, R. P. Van Duyne and J. T. Hupp, *Chem. Rev.*, 2012, **112**, 1105; (*c*) A. Barba-Bon, A. M. Costero, S. Gil, M. Parra, J. Soto, R. Martinez-Manezac and F. Sancenon, *Chem. Commun.*, 2012, **48**, 3000; (*d*) G. S. Yang, M. N. Li, S. L. Li, Y. Q. Lan, W. W. He, X. L. Wang, J. S. Qin and Z. M. Su, *J. Mater. Chem.*, 2012, **22**, 17947.

17 A. J. Lan, K. Li, H. H. Wu, D. H. Olson, T. J. Emge, W. Ki, M. C. Hong and J. Li, *Angew. Chem., Int. Ed.*, 2009, **48**, 2334.

18 S. R. Zhang, D. Y. Du, J. S. Qin, S. J. Bao, S. L. Li, W. W. He, Y. Q. Lan, P. Shen and Z. M. Su, *Chem. – Eur. J.*, 2014, **20**, 3589.

19 (*a*) X. Z. Song, S. Y. Song, S. N. Zhao, Z. M. Hao, M. Zhao, X. Meng, L. L. Wu and H. J. Zhang, *Adv. Funct. Mater.*, 2014, **24**, 4034; (*b*) D. K. Singha, P. Majee, S. K. Mondal and P. Mahata, *Eur. J. Inorg. Chem.*, 2015, 1390.

20 Z.-Q. Shi, Z.-J. Guo and H.-G. Zheng, *Chem. Commun.*, 2015, **51**, 8300.

21 M. Formica, V. Fusi, L. Giorgi and M. Micheloni, *Coord. Chem. Rev.*, 2012, **256**, 170.

22 K. Nakamoto, *Infrared and Raman Spectra of Inorganic and Coordination Compounds*, Wiley, New York, 4th edn, 1986, p. 231.

23 (*a*) J. L. McHale, *Molecular Spectroscopy*, Pearson Education (US), Upper Saddle River, 1998; (*b*) K.-A. Yao and D.-S. Zhao, *Instrumental Analysis*, Nanjing University, Nanjing, 2014; (*c*) S. Galli, A. Maspero, C. Giacobbe, G. Palmisano, L. Nardo, A. Comotti, I. Bassanetti, P. Sozzanic and N. Masciocchia, *J. Mater. Chem. A*, 2014, **2**, 12208.

24 X. L. Sun, Z. J. Wang, S. Q. Zang, W. C. Song and C. X. Du, *Cryst. Growth Des.*, 2012, **12**, 4431.

25 (*a*) R. K. Mane, B. D. Ajalkar and P. N. Bhosale, *Mater. Chem. Phys.*, 2003, **82**, 534; (*b*) M. Kaur and C. M. Nagaraja, *RSC Adv.*, 2014, **4**, 18257; (*c*) J. Guo, J. F. Ma, B. Liu, W. Q. Kan and J. Yang, *Cryst. Growth Des.*, 2011, **11**, 3609; (*d*) J. Li, X. Du, L. Yao and Y. Zhang, *Mater. Lett.*, 2014, **121**, 44; (*e*) F. Dong, Z. Zhao, T. Xiong, Z. Ni, W. Zhang, Y. Sun and W.-K. Ho, *ACS Appl. Mater. Interfaces*, 2013, **5**, 11392; (*f*) T. Wen, D.-X. Zhang, J. Liu, R. Lin and J. Zhang, *Chem. Commun.*, 2013, **49**, 5660; (*g*) M. Kaur, N. K. Gupta and C. M. Nagaraja, *CrystEngComm*, 2015, **17**, 2359; (*h*) Y. Zhao, Y. Zhang, L. Yao and M. Zhang, *Mater. Lett.*, 2014, **130**, 104; (*i*) T. Wang, Y. Zhang and T. Ding, *Mater. Lett.*, 2014, **123**, 153.

26 L. N. Li, S. Y. Wang, T. L. Chen, Z. H. Sun, J. H. Luo and M. C. Hong, *Cryst. Growth Des.*, 2012, **12**, 4109.

27 (*a*) S. J. A. Pope, B. J. Coe, S. Faulkner, E. V. Bichenkova, X. Yu and K. T. Douglas, *J. Am. Chem. Soc.*, 2004, **126**, 9490; (*b*) X.-L. Hu, C. Qin, X.-L. Wang, K.-Z. Shao and Z.-M. Su, *New J. Chem.*, 2015, **39**, 7858.

28 (*a*) S.-L. Zheng, J.-M. Yang, X.-L. Yu, X.-M. Chen and W.-T. Wong, *Inorg. Chem.*, 2004, **43**, 830; (*b*) S.-L. Zheng, M.-L. Tong, S.-D. Tan, Y. Wang, J.-X. Shi, Y.-X. Tong, H.-K. Lee and X.-M. Chen, *Organometallics*, 2001, **20**, 5319.

29 (*a*) S. S. Nagarkar, B. Joarder, A. K. Chaudhari, S. Mukherjee and S. K. Ghosh, *Angew. Chem., Int. Ed.*, 2013, **52**, 2881; (*b*) S. S. Nagarkar, B. Joarder, A. K. Chaudhari, S. Mukherjee and S. K. Ghosh, *Angew. Chem., Int. Ed.*, 2013, **125**, 2953.

30 P. Schwerdtheger, G. A. Heath, M. Dolg and M. A. Bennett, *J. Am. Chem. Soc.*, 1992, **114**, 7518.

31 K. Byriel, K. R. Dunster, L. R. Gahan, C. H. L. Kennard, J. L. Latten, I. L. Swann and P. A. Duckworth, *Polyhedron*, 1992, **11**, 1205.

32 S. K. Sahoo, D. Sharma, R. K. Bera, G. Crisponi and J. F. Callan, *Chem. Soc. Rev.*, 2012, **41**, 7195.

33 (*a*) X. H. Zhou, L. Li, H. H. Li, A. Li, T. Yang and W. Huang, *Dalton Trans.*, 2013, **42**, 12403; (*b*) J. Liu, Y. Zhong, P. Lu, Y. Hong, J. W. Y. Lam, M. Faisal, Y. Yu, K. S. Wong and B. Z. Tang, *Polym. Chem.*, 2010, **1**, 426; (*c*) B. Valeur, *Molecular Fluorescence: Principle and Applications*, Wiley-VCH, Weinheim, 2002; (*d*) S. Ramachandra, Z. D. Popović, K. C. Schuermann, F. Cucinotta, G. Calzaferri and L. De Cola, *Small*, 2011, **7**, 1488.

34 F. Hu, Y. X. Shi, H. H. Chen and J. P. Lang, *Dalton Trans.*, 2015, **44**, 18795.

35 (*a*) M. Guo and Z.-M. Sun, *J. Mater. Chem.*, 2012, **22**, 15939; (*b*) H. D. Xiao, J. H. Li, J. Zhao, G. Yin, Y. W. Quan, J. Wang and R. Y. Wang, *J. Mater. Chem. B*, 2015, **3**, 1633; (*c*) H. F. Xu, X. Zhu, H. Z. Ye, L. S. Yu, X. X. Liu and G. N. Chen, *Chem. Commun.*, 2011, **47**, 12158.

36 (*a*) B. L. Chen, S. G. Xiang and G. D. Qian, *Acc. Chem. Res.*, 2010, **43**, 1115; (*b*) M. D. Allendorf, C. A. Bauer, R. K. Bhakta and R. J. T. Houk, *Chem. Soc. Rev.*, 2009, **38**, 1330; (*c*) H. Xu, F. Liu, Y. J. Cui, B. L. Chen and G. D. Qian, *Chem. Commun.*, 2011, **47**, 3153.

37 (*a*) R. Wang, X. Liu, A. Huang, W. Wang, Z. Xiao, L. Zhang, F. Dai and D. Sun, *Inorg. Chem.*, 2016, **55**, 1782; (*b*) Y.-Q. Wang, Q.-H. Tan, H.-T. Liu, W. Sun and Z.-L. Liu, *RSC Adv.*, 2015, **5**, 86614; (*c*) W. Wang, J. Yang, R. Wang, L. Zhang, J. Yu and D. Sun, *Cryst. Growth Des.*, 2015, **15**, 2589.

38 (*a*) J. F. Ma, J. Yang, G. L. Zheng, L. Li and J. F. Liu, *Inorg. Chem.*, 2003, **42**, 7531; (*b*) X. Liu, Y. Zhang and B. Li, *J. Suzhou Univ. (Nat. Sci.)*, 2005, **121**, 59; (*c*) Y. H. So, *Macromolecules*, 1992, **25**, 516.

39 C. F. Macrae, I. J. Bruno, J. A. Chisholm, P. R. Edgington, P. McCabe, E. Pidcock, L. Rodriguez-Monge, R. Taylor, J. van de Streek and P. A. Wood, *J. Appl. Crystallogr.*, 2008, **41**, 466.

40 G. M. Sheldrick, *SHELXL 97. Programs for Crystal Structure Analysis (Release 97-2)*, University of Götinggen, Germany, 1997.

41 (*a*) E. L. Que, D. W. Domaille and C. J. Chang, *Chem. Rev.*, 2008, **108**, 1517; (*b*) Y. Y. Xiao, G. D. Qian and B. L. Chen, *Chem. Commun.*, 2010, **46**, 5503.